



Activating dinitrogen for chemical looping ammonia synthesis: Mn nitride layer growth modeling

Wrya Mohammadi Aframehr, Peter H. Pfromm *

Washington State University, Voiland School of Chemical Engineering and Bioengineering, 1505 Stadium Way, Pullman, WA 99164-6516, USA



HIGHLIGHTS

- Chemical looping ammonia synthesis (CLAS) based on Mn/Mn nitride.
- The dynamic process of bulk Mn nitridation has been investigated.
- Nitride layer growth was modeled by Reaction-diffusion and Internal oxidation models.
- N diffusion coefficient D_N , reaction rate K , and Damköhler # Da_{II} were estimated.
- Mass transfer in the solid is the limiting parameter in the Mn/Mn nitride based CLAS.

ARTICLE INFO

Article history:

Received 5 August 2021

Received in revised form 1 November 2021

Accepted 15 November 2021

Available online 18 November 2021

Keywords:

Manganese nitride

Ammonia synthesis

Chemical looping

N diffusion coefficient (D_N)

Reaction rate constant (K)

Mass transfer

ABSTRACT

The earth-abundant transition metal manganese (Mn) has been shown to activate dinitrogen (N_2) and store nitrogen (N) as nitride for subsequent chemical reaction, for example, to produce ammonia (NH_3). Chemical looping ammonia synthesis (CLAS) is a practical way to use Mn nitride by contacting nitride with gaseous hydrogen (H_2) to produce ammonia (NH_3). Here, the dynamic process of N atoms penetrating into solid Mn has been investigated. Nitride layer growth was modeled to quantify and predict the storage of activated N in Mn towards designing CLAS systems. The N diffusion coefficient (D_N) and reaction rate constant K for the first-order nitridation reaction were estimated at $6.2 \pm 5.5 \times 10^{-11} \text{ m}^2/\text{s}$ and $4.1 \pm 3.5 \times 10^{-4} \text{ 1/s}$, respectively, at atmospheric pressure and 700 °C. Assuming spherical particles of Mn with a diameter of $< 10 \mu\text{m}$, about 56.8 metric tons of Mn is sufficient to produce a metric ton of NH_3 per day using CLAS.

© 2021 Elsevier Ltd. All rights reserved.

1. Introduction

Affordable synthetic ammonia (NH_3) is emerging as a renewable energy carrier besides the fact that about 180 million metric tons of NH_3 are synthesized annually to enable the production of nearly half of the food that we eat. Traditional Haber-Bosch type processes based on natural gas or coal, and steam reforming to obtain hydrogen may have to be modified if the fossil carbon dioxide (CO_2) footprint of about 2.5% of global annual fossil CO_2 emission is to be reduced by shifting to renewable energy (Pfromm, 2017). The Haber-Bosch process can be modified with renewable hydrogen from electrolysis. However, intermittently available renewable hydrogen and more remote locations may call for an alternative to the high temperature/high pressure Haber-Bosch approach. An alternative method to produce NH_3 at atmospheric

pressure and elevated temperature is chemical looping ammonia synthesis (CLAS). As reported elsewhere (Aframehr et al., 2020; Aframehr and Pfromm, 2021) this method consists of converting the bulk of a fixed bed of solid manganese (Mn) particles to Mn nitrides by contacting with N_2 gas at atmospheric pressure and elevated temperature. Then by switching the gas from N_2 to H_2 over the nitrated Mn, NH_3 is produced at atmospheric pressure and elevated temperature. The looping process is completed by again nitrating the now partially N depleted Mn (Aframehr et al., 2020). The rationale for the choice of Mn as the solid for CLAS is that a balance must be struck between the activation of dinitrogen and absorption of N into the solid, and the subsequent activation of dihydrogen at the solid surface, and release of N atoms from the solid to produce NH_3 . Thermodynamic considerations to arrive at the choice of Mn can be found in previous publications (Michalsky et al., 2015c; Michalsky et al., 2015a; Michalsky and Pfromm, 2012).

* Corresponding author.

E-mail address: peter.pfromm@wsu.edu (P.H. Pfromm).

In this study, phenomenological modeling of nitride formation from solid Mn and gaseous N_2 via splitting of N_2 at the gas/solid interface followed by simultaneous diffusion of N atoms into the solid and reaction with Mn is attempted. The ultimate goal is to provide design parameters for a CLAS system.

Nitridation of metals in general and in particular of iron is well known and thoroughly described (Hekker et al., 1985; Jespersen et al., 2016; Lengauer et al., 1997; Van Wiggan et al., 1985) while nitridation of Mn has attracted much less attention in the published literature. This might be expected due to the numerous applications of iron and iron-containing materials and their interactions with nitrogen. This dearth of information is especially true for the non-steady state processes such as nitridation progressing from the solid-gas interface into the depth of metals in general, and Mn in particular, as will be discussed in the brief literature review below.

A study regarding modeling of nitriding in the Fe-M binary system (M being a placeholder for metals) is available as an example of the significant interest in Fe (Tomio et al., 2016a). In this study, alloy nitride precipitation during nitriding is developed and modeled for the Fe-M system. Number density, average radius, and volume fraction of alloy nitrides as a function of depth from the surface and nitriding time can be predicted by the model (Tomio et al., 2016a). Here we are adapting some of this work to Mn.

A few studies of Mn nitride are available (Heidlage et al., 2017a; Kropp et al., 2012; Michalsky and Pfromm, 2011; Shan et al., 2018, 2020; Wang et al., 2019; Buc, 2016; Liu et al., 2018), however, none of them focused on N diffusion in the solid and mathematical models of N penetration. Time dependent work is available on Mn nitridation only for extended nitridation times (Zhang et al., 2008). Although a kinetic model was developed for nitriding, N mass transfer and nitride layer growth quantification is not covered. In another study, Leineweber et al. investigated the crystal structures of select regions of the Mn-N phase diagram (Leineweber et al., 2004). Nevertheless, no detailed information was provided about the nitride layer and N diffusion into the solid with the simultaneous reaction of N with Mn. Niewa and coworkers studied Mn compounds, phases, and structures formed including structures, properties of the compounds, intermediate phases in the binary system Mn-N, and properties of ternary and higher Mn nitrides (Niewa, 2002). However, N mass transfer and modeling of nitride formation were not a target. Lassiri et al. focused on Mn nitride based materials as nitrogen transfer reagents for nitrogen chemical looping (Laassiri et al., 2018). Lattice nitrogen reactivity in different Mn nitride compositions was investigated. Elsewhere, Mn nitride was utilized for NH_3 synthesis, where the molecular-level pathway of the Mn nitride reduction was the subject (Shan et al., 2018). Michalsky et al. studied the hydrogenation of Mn nitrides during NH_3 production (Michalsky et al., 2015c; Michalsky et al., 2015a), and Heidlage et al. investigated the transformation of Mn nitride phases as a function of time and temperature (Heidlage et al., 2017a). To summarize, none of the studies above addressed the non-steady state N mass transfer and modeling of nitride formation in bulk solid Mn.

In our previous study, a two-step chemical looping process operating under relatively mild conditions to produce NH_3 was studied regarding Mn nitride phases and the particle surface morphology and composition (Aframehr et al., 2020). The time and temperature dependencies of Mn nitride layer growth and diffusion zone growth (microstructural development) during nitridation were investigated (Aframehr and Pfromm, 2021). The work presented here extends previous studies towards examining the non-steady state nitridation process as an N diffusion/reaction process and mathematical modeling of Mn nitride layer formation.

The overall goal of this work is to contribute to the understanding and quantification of non-steady state nitride formation from

solid Mn and gaseous N_2 via splitting of N_2 at the gas/solid interface, followed by simultaneous diffusion of N atoms into the solid and reaction with Mn. This is the first step in a chemical looping approach to synthesize NH_3 by subsequently contacting Mn nitride with gaseous H_2 (Aframehr et al., 2020; Aframehr and Pfromm, 2021). This looping NH_3 synthesis process is quite unique in that N atoms emanating from the bulk nitride react with hydrogen from the gas phase at the solid/gas interface. Reference experiments where a mixture of H_2 and N_2 is contacted with Mn at identical conditions showed, as expected, no NH_3 formation. This demonstrates that activation of dinitrogen by bulk nitride formation is fundamentally different from the conventional heterogeneous catalysis process where N_2 and H_2 are activated at the gas/solid interface to react (Marakatti and Gaigneaux, 2020; Somorjal and Zaera, 1982).

The present work aims to model the dynamic processes during gas/solid Mn nitridation. Simultaneous N penetration and chemical reaction taking place in the solid Mn are considered. Experimental results are compared to an internal oxidation model, and a Reaction-Diffusion model to predict storage of atomic nitrogen in Mn as a function of time.

2. Materials and Methods:

Manganese metal (Mn) plates (No. 36215, 0.8–12 mm, 99.98% pure (metals basis)) and Mn powder (No. 45089, average particle size < 10 μm , 99.6% pure) were from Alfa Aesar (No. 36215, 0.8–12 mm, 99.98% pure (metals basis)). Some inductively coupled plasma (ICP) analyses of technical grade Mn used in nitridation experiments revealed nickel (Ni) as a detectable low level impurity (fraction of a milligram Ni per gram of as-received Mn). Scanning electron micrographs (SEM) of as-received materials are shown in Fig. 1. The experimental setup was used as shown and described in our previous publication (Aframehr and Pfromm, 2021). A digital flow controller (Teledyne Hastings Instruments HFC-D-302B(H), Teledyne Hastings, Hampton, VA, U.S.A.) was used to control gas flow, in addition, a bubble flowmeter was used to check the flow. A tube furnace (Thermo Scientific Lindberg/Blue M, No. STF54434C) with quartz tubes (inner diameter 45 mm, Technical Glass Products Inc., No. 45X48) was used for running the thermochemical process. Quartz tubes were customized via glass blowing by narrowing on the inlet side to attach the gas feed and provided with custom end caps. Compressed dinitrogen (N_2 , ultra-high purity) and helium (He, ultra-high purity) were supplied by A-L Compressed Gases Inc. (99.999% purity, Spokane, WA, USA). All gas handling manifolds were constructed from Swagelok stainless steel fittings and tubing (1/8 in., Swagelok, S. Kent, Washington).

For each nitridation experiment, about 1 g of solid Mn was loaded into a combustion boat (Cooresk Inc. No. 65568). Samples were always dried in an oven (Thermo Scientific Lindberg/Blue M, No. VO1218A-1) at 100 °C for about 60 min in air. The dried loaded boat was then placed in the center of the furnace tube after weighing (Mettler Toledo, No. MS204S/03, ± 0.00005 g). N_2 gas (1 cm^3 (-Standard Temperature and Pressure, STP)/s, STP: 1 bar, 0°C) was directed over the sample at 100 °C for about 10 h as pre-process in situ drying. The furnace tube was then purged with N_2 gas at a flow of 2 cm^3 (STP)/s and heated to 700 °C. Cooldown was under 2 cm^3 (STP)/s N_2 at the end of the experiment. All processing was at atmospheric pressure. After nitridation, weight and SEM (with EDX) were obtained. The possible impact of the size and shape of the load in the boat was ruled out through reference experiments with different loading in the boat (not shown).

The choice of 700 °C for this work is guided by previous work where the impact of temperature on the different nitride phases

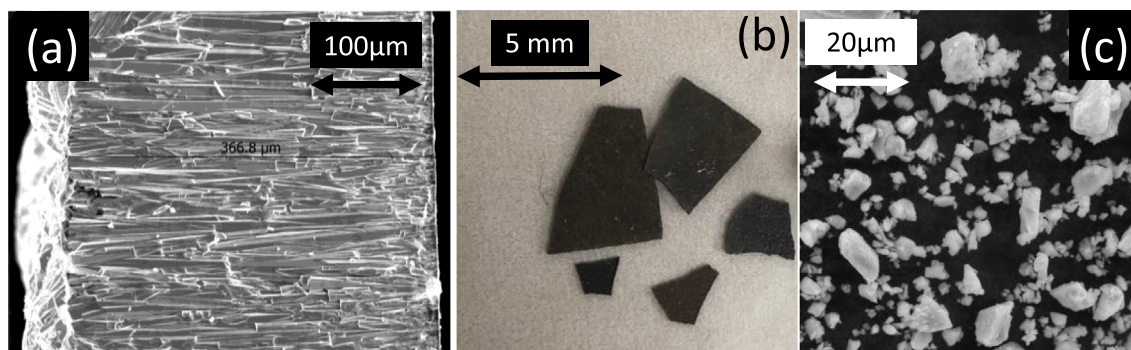


Fig. 1. As-received material: SEM images of Mn plate cross-section, (a), an overview image of Mn plate (b), and Mn powder (c).

that are formed was investigated (Aframehr et al., 2020; Heidlage et al., 2017a)

Parasitic oxygen (O_2) could enter the reactor with the sample, the combustion boat, or through leaks. The strong tendency of Mn to oxidize would lead to the formation of oxides on the Mn surface. A reference experiment was therefore conducted with identical conditions as in nitridation, but helium (He) instead of N_2 . The parasitic oxygen weight gain from a He purged experiment was subtracted from the apparent nitridation weight gain. In 4-hour nitridation experiments, the weight gain was in one example 0.01295 ± 0.00007 g/g Mn. However, reference experiments using He showed that 0.00074 ± 0.00007 g/g Mn was due to parasitic oxygen. The N weight gain was therefore calculated by difference as 0.01221 ± 0.0001 g/g Mn.

The temperature as a set at the furnace controller exceeded the actual temperature in the sample boat by a maximum of 17 °C as determined using a thermocouple (Omega/CL3515R). Heat up and cool down are described by Eq. (1) and (2) respectively (tube furnace nitridation procedure shown in our previous work (Aframehr and Pfromm, 2021)).

$$T = 63.86t_m + 59.03 \quad (1)$$

$$T = 698.58e^{-0.016t_m} \quad (2)$$

where T (°C) and t_m (min) are furnace controller setpoint temperature and time, respectively.

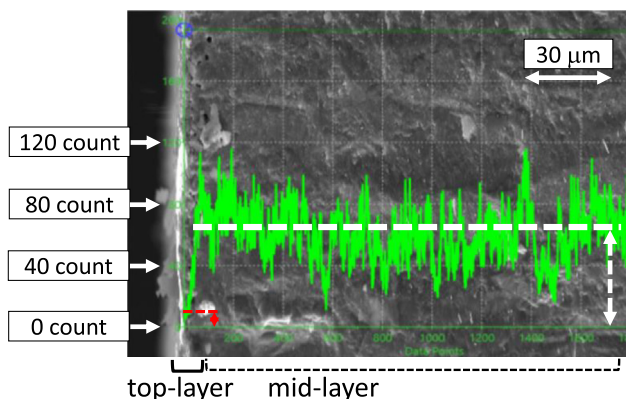


Fig. 2. The EDX line spectra of Mn nitride cross-sectional view. Estimation of the surface N content (wt%) in Mn plates during nitridation by assuming 1.22 ± 0.01 wt% N weight gain, and that essentially all N is stored in the mid-layer. The N concentration at the surface (C_N^S) is estimated as 0.18 ± 0.06 wt%.

2.1. N Concentration on the top-layer (C_N^S)

The N concentration on the exterior solid surface termed “top-layer” (C_N^S , wt%, Fig. 2) is important for the modeling of Mn nitridation. Due to the low N concentration in the surface, C_N^S is not directly and quantitatively measurable with the equipment and methods used here. C_N^S was therefore estimated relative to the independently known (via mass uptake) N concentration and N penetration depth in the mid-layer (Fig. 2). The total N mass uptake of Mn plates was 1.22 ± 0.01 wt% determined by weighing (Mettler Toledo, No. MS204S/03, ± 0.00005) of an Mn plate (about 1 g) before and after a representative nitridation experiment. Since the surface of the plate consists largely of MnO (Aframehr et al., 2020) and assuming all N essentially is stored in the mid-layer for plate nitridation, one can estimate;

$$C_N^S = (\varphi/\omega) \times C_N^M \quad (3)$$

where C_N^S (wt%) is the N concentration in the top-layer (on the exterior surface), φ (count) is the measured count when scanning the top-layer by EDX, and ω (count) is the N count in the mid-layer (see Fig. 2). The C_N^M (wt%) is the N concentration in the mid-layer equal to 1.22 ± 0.01 wt% as calculated from mass balance. C_N^S is estimated at about 0.18 ± 0.06 wt% using measured values of $\varphi = 10.6 \pm 1.5$, and $\omega = 70 \pm 20$ counts, respectively which is represented in Fig. 2.

3. Results and discussion:

The diffusion coefficient of N in Mn will first be estimated after discussing some definitions and assumptions. Two models will then be applied to describe experimental data: the internal oxidation model (Tomio et al., 2016a) and the Reaction-Diffusion (Fick's second law with irreversible first order reaction). The reaction rate coefficient, k for the first-order reaction is estimated here. It will be shown that mass transfer via diffusion of N in Mn is the limiting process (see Fig. 8) in quantifying the extent of nitridation (nitridation depth) of solid Mn exposed to gaseous N_2 at 700 °C and atmospheric pressure.

3.1. Definitions and assumptions

Fig. 3 shows a snapshot of the dynamic process of N atoms penetrating into solid Mn. This is an attempt to visualize the situation in the solid at a given time of exposure of Mn to gaseous N_2 at 700°C. This was accessed experimentally by cooling an Mn sample after exposure to N_2 , followed by fracturing and imaging the interior cross-section (Aframehr and Pfromm, 2021). It is assumed that

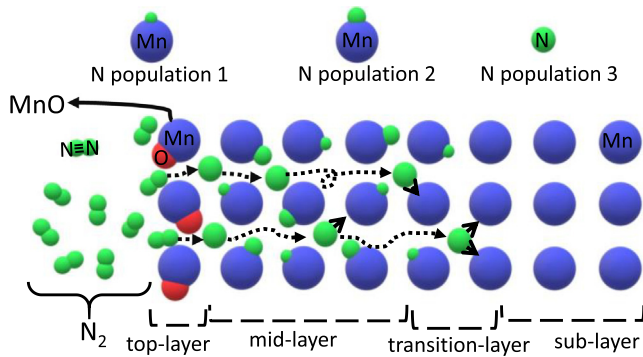


Fig. 3. Simplified schematic of the Mn nitridation process which shows N populations in a simplified Mn nitride lattice. N atoms are shown with different sizes to facilitate identification. Immobile Mn oxide is shown at the Mn surface (Aframehr and Pfromm, 2021).

N_2 molecules are split at the solid surface and then migrate as N atoms into the solid.

3.1.1. Nitrogen populations

The Mn is over time converted to nitrides when exposed to dinitrogen at 700 °C and atmospheric pressure. Three different populations of N in Mn were postulated. This was supported via WAXD, EDX, electron microscopy, and mass balance (Aframehr et al., 2020; Aframehr and Pfromm, 2021):

Population 1: atomic nitrogen that is strongly bonded (for the definition of ‘strong’ and ‘weak’ Mn-N interaction, see (Mittemeijer and Somers, 2015)) to Mn. Evidence of strong bonding is also that this N can not be harvested in the subsequent hydrogenation step at 700 °C to produce NH_3 . Population 1 is about 57 atom % of the nitrogen present as nitrides based on the NH_3 harvesting yield (24 h, 700 °C).

Population 2: atomic N that is bonded by a covalent/ionic hybrid bond. As a result, population 2 can be harvested relatively easily during exposure to H_2 for NH_3 harvesting.

Population 3: atomic N that does not bond to Mn. This population resides in imperfections of the Mn lattice. Population 3 can diffuse through existing nitride towards the bulk.

We have adopted general models to describe diffusion and the reaction of N with solid Mn to make quantitative predictions of N penetration in Mn. Generally, the dynamics of the moving reaction/diffusion front as N penetrates into Mn are the result of the competition between mass transfer in the gas phase and the solid, adsorption and reaction (N_2 splitting) at the solid/gas interface, and reactions of N with Mn to form nitrides. However, N diffusion in Mn governs the process in the case of Mn nitridation as will be shown below. The reason is the low N diffusion coefficient even at elevated temperatures (see Fig. 8).

3.2. Estimating the diffusion coefficient

The classical solution to the one-dimensional diffusion of a penetrant through a solid matrix with a constant diffusion coefficient is applied (Crank, 1975).

$$Q_t = D(C_1 - C_2) \frac{t}{L} + \frac{2L}{\pi^2} \sum_{n=1}^{\infty} \frac{C_1 \cos n\pi - C_2}{n^2} \left[1 - \exp\left(-\frac{Dn^2\pi^2 t}{L^2}\right) \right] + \frac{4C_0 L}{\pi^2} \sum_{m=0}^{\infty} \frac{1}{(2m+1)^2} \left[1 - \exp\left(-\frac{D(2m+1)^2\pi^2 t}{L^2}\right) \right] \quad (4)$$

where, Q_t (mol/m²) is the total amount of diffusing substance per unit surface of a semi-infinite plate at time t (s), and C_0 , C_1 and C_2 (mol/m³) are the initial, feed side, and permeate side concentrations in the plate, respectively (Fig. 4). L (m), and D (m²/s), are the thick-

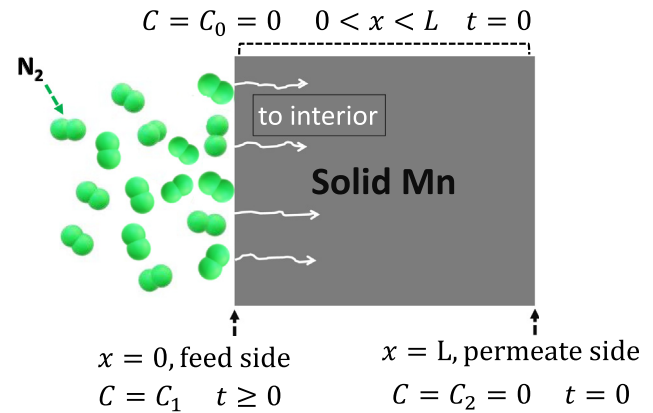


Fig. 4. Schematic of one-dimensional N atom diffusion during Mn plate nitridation. The schematic shows the physical characteristics and boundary conditions.

ness of the plate, and the diffusion coefficient, respectively (Crank, 1975).

At infinite time, and assuming that the initial concentration in the solid is equal to zero ($C_0 = C_2 = 0$) Eq. (4) takes the form;

$$Q_t = (DC_1/L)t - (LC_1/6) \quad (5)$$

By plotting experimental data for Q_t vs. t (Aframehr and Pfromm, 2021) for nitridation of Mn, D can be derived from the slope (Eq. (6)).

$$Q_t = (9 \times 10^{-5})t - 0.221 \quad (6)$$

Applying Eq. (6), the slope is 0.00009 (mol/m²) by considering the nitrogen concentration on the feed side as surface concentration (C_1). The nitrogen diffusion coefficient (D_N) is about $6.2 \pm 5.5 \times 10^{-11}$ (m²/s). This appears reasonable compared to similar systems (Bobadilla and Tschiptschin, 2015; Zhang et al., 2010).

The diffusion coefficient D_N will now be used to model simultaneous N transport and reaction in Mn.

3.3. Gas-solid nitridation

Consider a general gas–solid nitridation at elevated temperature and atmospheric pressure:



where a and b depend on nitride phases as identified based on XRD (Aframehr et al., 2020). K is the reaction rate coefficient and s and g indicate solid and gas, respectively.

Eq. (8) describes simultaneous reaction–diffusion (Kuttler, 2011):

$$u_t = D\Delta u + f(u) \quad (8)$$

where $u = u(x, t)$ is a state variable and describes the concentration of the diffusing substance, at position x (m) and at time t (s). Δ and D denotes the Laplace operator and diffusion coefficient. The first term on the right hand side describes the diffusion while the second term, $f(u)$ is a smooth function $f: r \rightarrow r$ that describes processes such as production or consumption via a chemical reaction.

The reaction–diffusion equation (Eq. (8)) in one dimension (diffusion/reaction into an infinite plate) is investigated here for Mn nitridation at elevated temperature and atmospheric pressure.

3.4. Diffusion occurring with a first-order reaction

The reaction of N with Mn is assumed to be an irreversible first-order reaction (King et al., 2018; Vasquez et al., 1986). Diffusion

occurring with an irreversible first-order reaction can be described by (Crank, 1975);

$$\frac{\partial C}{\partial t} = D \frac{\partial^2 C}{\partial x^2} - KC \quad (9)$$

where K (1/s) is a first-order rate constant for the reaction, and C is the concentration (mol/m³). In general, Eq. (9) cannot be solved analytically, however, numerical solutions can be obtained (Biology and Cobi, n.d.; Page, 2007). The Crank-Nicolson method (Page, 2007) is applied here to solve Eq. (9) and the result is plotted in Fig. 8.

3.5. Diffusion only

Simplifying in one dimension and focusing on the diffusion of N only;

$$\frac{\partial C}{\partial t} = D \frac{\partial^2 C}{\partial x^2} \quad (10)$$

Analytical and approximate solutions of this equation are available (Crank, 1975; Rezzolla, 2020).

3.6. Diffusion with absorption

By considering absorption, the amount of diffusing N absorbed in a unit volume of solid Mn is proportional to its free concentration. If S is the concentration of immobilized N and R is the constant of proportionality (Crank, 1975), so that $S = RC$, then the diffusion equation (Crank, 1975);

$$\frac{\partial C}{\partial t} = D \frac{\partial^2 C}{\partial x^2} - \frac{\partial S}{\partial t} \quad (11)$$

By substituting S with RC , this equation can be rearranged to the same form as the basic equation for free diffusion but with an effective diffusion coefficient D_N^{mod} given by (Crank, 1975);

$$D_N^{mod} = D \frac{1}{R+1} \quad (12)$$

3.7. Internal oxidation model applied to nitridation of Mn

The internal oxidation model by Lightfoot and Jack (Lightfoot and Jack, 1975; Tomio et al., 2016a) was selected to predict the depth of the nitride layer in solid Mn with time. In this model, the following assumptions are considered:

1. The diffusion of Mn atoms is neglected.
2. The atomic nitrogen concentration at the dinitrogen gas/solid interface is constant.
3. The Mn solid is uniform.
4. The N diffusion coefficient (D_N) is constant.

A mass balance of N over the transition layer is (Tomio et al., 2016a);

$$nC_{Mn}^0 \frac{\partial x}{\partial t} = D_N \frac{\partial C_N}{\partial x} \quad (13)$$

where C_N and C_{Mn}^0 are the N and Mn concentrations in atom% (see Fig. 5). n is the ratio of N over Mn atoms. Based on WAXD, n is taken as 0.426 since Mn₆N_{2.56} is the most abundant phase for Mn nitrided at 700°C and atmospheric pressure (Aframehr et al., 2020).

3.7.1. Boundary conditions

At the dinitrogen gas–solid interface, local equilibrium between the gas and the solid surface where dinitrogen is being dissociated

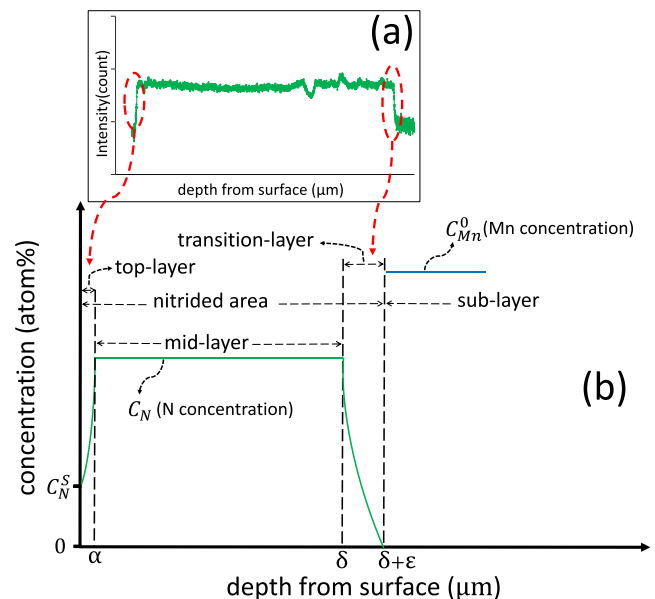


Fig. 5. (a) The EDX line spectra of Mn nitride (4 h nitridation at 700 °C) cross-sectional view. N atom trace shows the increase in N detected (top-to-mid-layer) and a decrease in N detected (mid-layer through transition-layer to unchanged Mn towards the interior of the plate, (see Fig. 6)). (b) concentration (atom%) profile schematic of N and Mn during Mn nitridation at 700 °C and atmospheric pressure based on EDX result (Fig. 6).

will be assumed. A nitrogen concentration of zero is assumed for the interior of the solid beyond the transition-layer. The Mn plate is considered semi-infinite so that nitridation is assumed to proceed from the surface towards the interior only.

Assuming a linear gradient of nitrogen in the near-surface top-layer

$$nC_{Mn}^0 \frac{\partial x}{\partial t} = D_N \frac{C_N^S}{x} \quad (14)$$

where C_N^S (atom%) is the N concentration at the surface of Mn. Integrating Eq. (14), and rearranging yields;

$$x(t) = \left(2C_N^S D_N t / nC_{Mn}^0 \right)^{1/2} \quad (15)$$

It seems impractical to assume that all Mn (Populations 1 and 2) is bonded instantaneously upon the arrival of N atoms. However, after some time, the dissolved N (Population 3) will likely reach its saturation level (see Fig. 5 and 6 mid-layer), and the maximum amount of N is now bonded to Mn (Populations 1 and 2). The nitriding front in the transition-layer advances further towards the interior of the Mn. In this study, the data from EDX and the total amount of N absorbed in the solid were used to predict the nitridation depth. The calculation of the concentration of N at the surface (C_N^S about 0.51 ± 0.30 atom%) is explained in detail in the materials and methods section.

Based on the EDX results (Aframehr and Pfromm, 2021), Fig. 5 shows the assumed profile of N and Mn concentration in the solid. The N concentration changes with distance from the surface. Four different zones are identified (Fig. 5 and 6): top-layer (local equilibrium with the dinitrogen gas/nitrogen atoms at the gas/solid interface labeled C_N^S , increasing to C_N at depth α), mid-layer (constant overall nitrogen concentration C_N , thickness $\delta-\alpha$), transition-layer (decreasing nitrogen concentration, thickness ϵ), and sub-layer (N is non-detect in EDX, Mn concentration C_{Mn}^0 representing solid α -Mn). It should be noted that a driving force for diffusion into the bulk Mn obviously exists since N uptake contin-

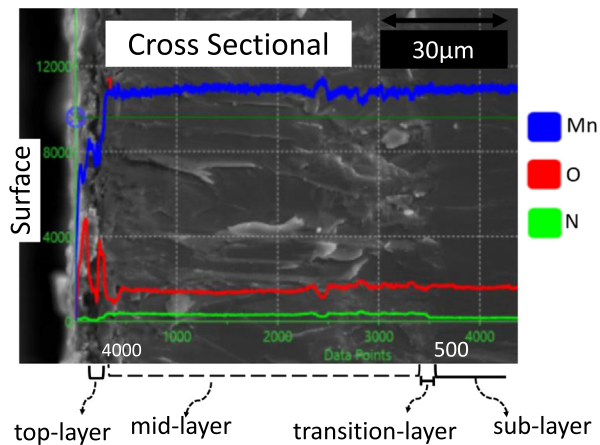


Fig. 6. The EDX line spectra of the solid Mn cross-sectional view after 4 h nitridation at 700 °C and atmospheric pressure. Nitridation produces two additional morphologies, coinciding with an increase of N detected (top-to-mid layer) and a decrease of N detected (mid-layer through transition-layer to unchanged Mn towards the interior of the plate). For more details about morphologies see previous work (Aframehr and Pfromm, 2021).

ues with time. The concentration increase from the top-layer to the mid-layer may seem to indicate that mass transfer should proceed from the mid-layer to the top-layer but the chemical potential difference as the underlying driving force for diffusion may well have the opposite direction due to the different properties of the top-layer (containing Mn oxide) and the bulk Mn and later Mn nitride in the deeper layers.

The diffusion coefficient D_N can then be used to attempt a fit of Eq. (15) to our experimental data.

3.8. Reaction-Diffusion model applied to nitridation of Mn

In the Mn nitridation process, a reaction will occur between N and Mn in addition to N diffusion. By applying the Reaction-Diffusion model, the depth of the nitride layer in solid Mn with time can be predicted under the following assumptions:

1. The reaction of dissolved nitrogen atoms with lattice Mn yields Mn nitrides and it is the only reaction.
2. Nitridation occurs at the interface between the nitrided and the non-nitrided regions.
3. The atomic nitrogen concentration at the dinitrogen gas/solid interface is constant.
4. The Mn solid is uniform.
5. The diffusion of Mn atoms is neglected.
6. N diffusion coefficient (D_N) and reaction rate (K) are constant.

A mass balance of N over the transition layer assuming a constant diffusion coefficient can then be described as ((Tomio et al., 2016a));

$$nC_{Mn}^0 \frac{\partial C}{\partial t} = D_N \frac{\partial^2 C}{\partial x^2} + KC \quad (16)$$

n is taken as 0.426 since $Mn_6N_{2.56}$ is the most abundant phase, based on WAXD. The terms in Eq. (16) represent from left to right, accumulation, diffusion, and reaction.

3.8.1. Boundary conditions

At the dinitrogen gas–solid interface, a local equilibrium between the gas and the solid surface where dinitrogen is being dissociated will be assumed. A linear gradient of N at the gas–solid interface is assumed. A nitrogen concentration of zero is assumed

for the interior of the solid beyond the transition-layer (Fig. 5). Again, the Mn plate is considered semi-infinite so that nitridation is assumed to proceed from the surface towards the interior only.

By assuming a linear gradient of nitrogen at the gas–solid interface ($\partial C/\partial x = C/x$)

$$nC_{Mn}^0 \frac{\partial C}{\partial t} = D_N \frac{\partial}{\partial x} \left(\frac{C}{x} \right) + KC \quad (17)$$

which can be solved to arrive at;

$$nC_{Mn}^0 \frac{\partial C}{\partial t} = C \left(K - \frac{D_N}{x^2} \right) \quad (18)$$

Integrating Eq. (18), and rearranging yields

$$x(t) = \left(D_N t / \left(K t - nC_{Mn}^0 \ln C_N^S \right) \right)^{1/2} \quad (19)$$

where C_N^S (atom%) is the N concentration at the surface of Mn (Fig. 5). In the reaction–diffusion case of nitridation at elevated temperature and atmospheric pressure, it seems reasonable to simplify steps occurring in the overall process (see Fig. 3):

- 1) Diffusion of N_2 from the bulk of the nitrogen gas to the interface between the gas and the solid.
- 2) The N_2 molecules are split into N atoms at the surface of the solid.
- 3) Diffusion of N within the solid.
- 4) Thermochemical reaction (N consumption) within the solid.

After some time, the dissolved N (Population 3) will likely reach its saturation level because of the reaction between N and Mn (see Fig. 5, mid-layer). The maximum amount of N is now bonded to Mn. However, because of the low D_N , diffusion dominates the nitridation process compared to chemical reaction (K). A kinetic reaction rate constant K for the first-order reaction can be estimated as $4.1 \pm 3.5 \times 10^{-4}$ 1/s comparing the reaction–diffusion equation (Eq. (19)) with the experimental results (Fig. 7).

3.9. Comparison of models

Table 1 shows the comparison of both internal oxidation and Reaction-Diffusion models boundary conditions, assumptions, advantages, and disadvantages. The listed parameters that occur in both models are of identical numerical value.

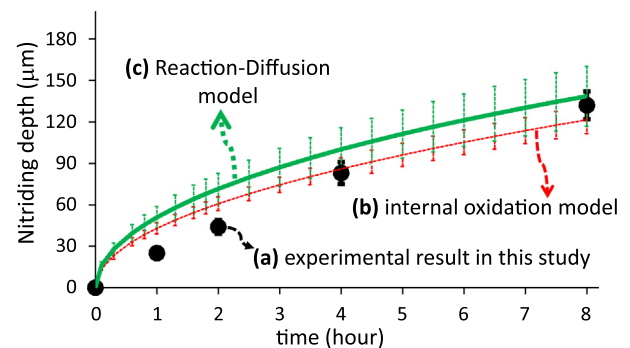


Fig. 7. The nitriding depth as a function of nitridation time, for (a, black circles with error bar) experimental data of a solid Mn plate, nitrided at 700°C and atmospheric pressure, (b, red line) predicted by the internal oxidation model (Eq. (15)), and (c, green line) predicted by the Reaction-Diffusion model (Eq. (19)) using the same diffusion coefficient estimate from mass uptake measurements, and estimating a first-order rate constant K for the nitridation reaction. The models are afflicted with errors based on the experimental data used to specify them. (For interpretation of the references to colour in this figure legend, the reader is referred to the web version of this article.)

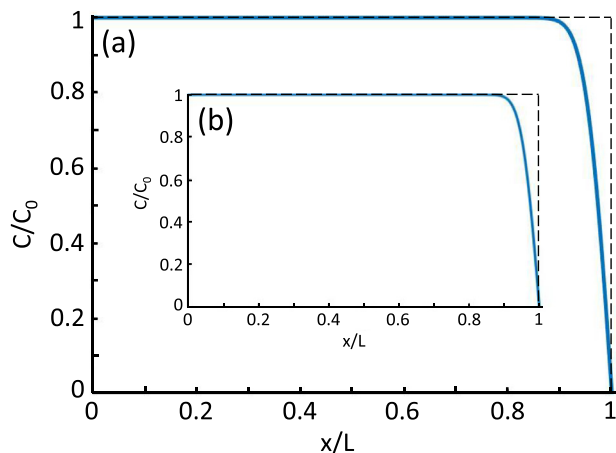


Fig. 8. Concentration profile at the transition-layer (where N encounters available Mn for the first time), (a) when reaction and diffusion occurs, and (b) when only diffusion occurs. Concentration profiles in both diffusion only and reaction-diffusion are similar since diffusion in the solid governs the Mn nitridation process. The profile was plotted based on the Crank-Nicolson method (Page, 2007) to solve the equation for diffusion occurring with a first-order reaction (Eq. (9)). D and K were utilized to plot based on calculations in this study.

3.10. Models versus experimental data

Fig. 7 compares experimental data with the internal oxidation and Reaction-Diffusion model using the diffusion coefficient calculated from the mass uptake of Mn at 700 °C and atmospheric pressure. The models appear to represent the data reasonably well. The internal oxidation model shows a somewhat superior fit. This supports the notion that diffusion controls the nitriding depth as a function of time rather than the chemical reaction taken in account for the Reaction-Diffusion model.

The somewhat increased nitriding depth relative to the experimental result could be attributed to

1. The presence of oxides in the top-layer (see previous work (Aframehr and Pfromm, 2021)) may result in a low amount of N population 3 at the beginning of nitridation (see Fig. 3).
2. The validity of some of the assumptions.

3.11. Modified Damköhler number (Da_{II}) to describe the mass transfer as the limiting issue

Both reaction and mass transport play an important role in Mn nitridation. Here the second Damköhler number (Da_{II}) is estimated to quantify which process is dominant, and to allow predictions if other materials are to be nitrided.

In reacting systems with interphase diffusion (mass transfer), the Damköhler number is the ratio of the characteristic mass trans-

fer time ($t_m = 1/(k_m a_r)$) and the characteristic reaction time ($t_r = 1/(k_r C_0^{s(j-1)})$) (Die et al., 1936; Kashid and Renken, 2015);

$$Da_{II} = \frac{\text{reaction rate}}{\text{diffusive mass transfer rate}} = \frac{\text{mass transfer time}}{\text{reaction time}} \quad (20)$$

$$Da_{II} = \frac{t_m}{t_r} = \frac{k_r C_0^{s(j-1)}}{k_m a_r} = \frac{k_r A C_0^{s(j-1)}}{D_N} = \frac{k_r A}{D_N} \quad (21)$$

where k_r and k_m are the first-order reaction rate constant (1/s) and the mass transfer coefficient (m/s), respectively, for homogeneous and quasi-homogeneous materials. j , a_r , and A are the reaction order, specific interfacial area per volume (m^2/m^3), and the interfacial area (m^2), respectively.

Based on estimated D_N and k_r and using the interfacial area (A) of the solid Mn, Da_{II} can be estimated as 2.97×10^3 which demonstrates that Mn nitridation at elevated temperature and atmospheric pressure is mass transfer limited.

3.12. CLAS scale-up

The results for micrometer-scale Mn powder ($<10 \mu\text{m}$, Fig. 1, C) nitridation show that after 4 h nitridation at 700 °C and atmospheric pressure, N weight gain is about 92.5 ± 9.3 kg N metric ton Mn^{-1} . Analyses in this paper and our previous study (Aframehr and Pfromm, 2021) confirm that of 100 stored N atoms in Mn as Mn nitride, about 17 N atoms are converted to NH_3 , with 57 N atoms remaining as a process deadload and the remainder lost as N_2 . After 20 h hydrogenation at 700 °C and atmospheric pressure in the CLAS, 17.6 ± 1.1 kg NH_3 metric ton $\text{Mn}^{-1} \text{day}^{-1}$ could be harvested. As reported previously a reactor (see Figure 16, (Aframehr and Pfromm, 2021)) with about 1.68 m^3 net volume of Mn as $<10 \mu\text{m}$ Mn particles could be used for the CLAS to produce about 17.6 ± 1.1 kg NH_3 per day. These particles could be deposited, for example, on the walls of a multichannel monolithic ceramic carrier, or deposited in a ceramic foam. An Mn monolith with multiple channels would be another geometry that might be explored since Mn is rather inexpensive.

4. Conclusions

The dynamic process of N atoms penetrating into solid Mn was described based on different N populations (Fig. 3). After estimating the diffusion coefficient of N in Mn based on experimental data, two phenomenological mathematical models were used to describe N penetration into a semi-infinite Mn plate. Diffusion and simultaneous reaction-diffusion were modeled.

Both the internal oxidation and Reaction-Diffusion model predict the nitridation depth as a function of time at 700 °C and atmospheric pressure well. Mass transfer of N was found to be the limiting process demonstrated by a calculation of the second

Table 1

The boundary conditions, assumptions, advantages, and disadvantages of the internal oxidation and Reaction-Diffusion models.

Model	Parameter	Boundary Condition	Assumption	Advantage	Disadvantage
Reaction-Diffusion	C_N^s	$x = 0 \ C = C_N^s$ for $t \geq 0$	1) $\text{N} + \text{Mn} = \text{Mn nitride}$, is the only reaction.	Consider reaction in nitridation	More assumptions apply
	D_N	$x = 0 \ \partial C/\partial x = C/x$ for $t \geq 0$	2) Nitridation occurs at the interface between the nitrided and the non-nitrided regions.		
	K	$x = L \ C = 0$ for $t = 0$	3) C_N^s is constant.		
	t	$0 < x < L \ C = 0$ for $t = 0$	4) Mn solid is uniform.		
	n		5) The diffusion of Mn atoms is neglected.		
Internal oxidation	C_{Mn}^0		6) D_N and K are constant.	Does not need additional parameters to apply	Neglect reaction
	C_N^s	$x = 0 \ C = C_N^s$ for $t \geq 0$	1) C_N^s is constant.		
	D_N	$x = 0 \ \partial C/\partial x = C/x$ for $t \geq 0$	2) Mn solid is uniform.		
	t	$x = L \ C = 0$ for $t = 0$	3) The diffusion of Mn atoms is neglected.		
	n	$0 < x < L \ C = 0$ for $t = 0$	4) D_N is constant.		

Damköhler number. Particle size is therefore the most important parameter to minimize cycle time for chemical looping of Mn to synthesize ammonia via the nitride route. The CLAS process is easily optimized by adjusting the Mn particle size while reactor design should focus on exposing the particles to the various gases perhaps in microchannels known from catalytic converters, or other supporting structures such as foams.

CRedit authorship contribution statement

Wrya Mohammadi Aframehr: Investigation, Methodology, Data curation, Formal analysis, Writing – original draft. **Peter H. Pfromm:** Conceptualization, Methodology, Supervision, Writing – review & editing, Funding acquisition.

Declaration of Competing Interest

The authors declare that they have no known competing financial interests or personal relationships that could have appeared to influence the work reported in this paper.

Acknowledgments

This research was supported by the National Science Foundation under Grant No. 1856084 for the FEWtures project. We gratefully acknowledge access to the Franceschi Microscopy and Imaging Center, L.J. Smith Hall, at Washington State University.

References

- Aframehr, W.M., Huang, C., Pfromm, P.H., 2020. Chemical Looping of Manganese to Synthesize Ammonia at Atmospheric Pressure: Sodium as Promoter. *Chem. Eng. Technol.* 43 (10), 2126–2133. <https://doi.org/10.1002/ceat.202000154>.
- Mohammadi Aframehr, W., Pfromm, P.H., 2021. Activating dinitrogen for chemical looping ammonia synthesis: nitridation of manganese. *J. Mater. Sci.* 56 (22), 12584–12595. <https://doi.org/10.1007/s10853-021-06079-7>.
- Biology, C., Cobi, G., n.d. Numerical Solution of reaction-diffusion problems 1–44.
- Bobadilla, M., Tschiptschin, A., 2015. On the nitrogen diffusion in a duplex stainless steel. *Mater. Res.* 18 (2), 390–394. <https://doi.org/10.1590/1516-1439.337714>.
- Buc, M.M., 2016. Convenient synthesis of nanocrystalline powders of phase-pure manganese nitride g -Mn 3 N 2 8177–8186. <https://doi.org/10.1007/s10853-016-0094-2>
- Crank, J., 1975. The mathematics of diffusion.
- Die, A.U.F., Reaktionsofen, LV.O.N., Damkohler, V.G., 1936. EINFLUSS DER STROMUNG. DIFFUSION LTND DES WARMEOBERGANGES AUF DIE LEISTUNG VON REAKTIONSOFFENNO Title, Wiley Online Libr.
- Heidlage, M.G., Kezar, E.A., Snow, K.C., Pfromm, P.H., 2017a. Thermochemical Synthesis of Ammonia and Syngas from Natural Gas at Atmospheric Pressure. *Ind. Eng. Chem. Res.* 56 (47), 14014–14024. <https://doi.org/10.1021/acs.iecr.7b03173>.
- Hekker, P.M., Rozendaal, H.C.F., Mittemeijer, E.J., 1985. Excess nitrogen and discontinuous precipitation in nitrided iron-chromium alloys. *J. Mater. Sci.* 20 (2), 718–729. <https://doi.org/10.1007/BF01026547>.
- Jespersen, F.N., Hattel, J.H., Somers, M.A.J., 2016. Modelling the evolution of composition-and stress-depth profiles in austenitic stainless steels during low-temperature nitriding. *Model. Simul. Mater. Sci. Eng.* 24 (2), 025003. <https://doi.org/10.1088/0965-0393/24/2/025003>.
- Kashid, M.N., Renken, A., 2015. Microstructured Devices for Chemical Microreactors in Organic Innovative Gates to Intensified and.
- King, P.L., Wheeler, V.M., Renggli, C.J., Palm, A.B., Wilson, S.A., Harrison, A.L., Morgan, B., Nekvasil, H., Troitzsch, U., Mernagh, T., Yue, L., Bayon, A., Difrancesco, N.J., Baile, R., Kreider, P., 2018. Gas – Solid Reactions : Theory, Experiments and Case Studies Relevant to Earth and Planetary Processes 84, 1–56.
- Kropp, H., King, A.E., Khushniyarov, M.M., Heinemann, F.W., Lancaster, K.M., DeBeer, S., Bill, E., Meyer, K., 2012. Manganese nitride complexes in oxidation states III, IV, and V: Synthesis and electronic structure. *J. Am. Chem. Soc.* 134 (37), 15538–15544. <https://doi.org/10.1021/ja306647c>.
- Kuttler, C., 2011. Reaction-Diffusion equations with applications.
- Laassiri, S., Zeinalipour-Yazdi, C.D., Catlow, C.R.A., Hargreaves, J.S.J., 2018. The potential of manganese nitride based materials as nitrogen transfer reagents for nitrogen chemical looping. *Appl. Catal. B Environ.* 223, 60–66. <https://doi.org/10.1016/j.apcatb.2017.04.073>.

- Leineweber, A., Jacobs, H., Kockelmann, W., 2004. Nitrogen ordering in ζ -manganese nitrides with hcp arrangement of Mn - MnNy with $0.39 < y < 0.48$ - Determined by neutron diffraction. *J. Alloys Compd.* 368, 229–247. <https://doi.org/10.1016/j.jallcom.2003.08.062>.
- Lengauer, W., Wiesenberger, H., Mayr, W., Bidaud, E., Berger, R., Ettmayer, P., 1997. Phase stabilities of transition metal carbides and nitrides investigated by reaction diffusion. *J. Chim. Phys. Physico-Chimie Biol.* 94, 1020–1025. <https://doi.org/10.1051/jcp/1997941020>.
- Lightfoot, B.J., Jack, D.H., 1975. Kinetics of nitriding with and without white-layer formation. *Heat Treat. Met. Soc London*, 30.
- Liu, B., Shan, N., Lee, R.T., Pfromm, P., 2018. Predicting the behavior of manganese nitrides for atmospheric ammonia synthesis 66506, 1726332.
- Marakatti, V.S., Gaigneaux, E.M., 2020. Recent Advances in Heterogeneous Catalysis for Ammonia Synthesis. *ChemCatChem* 12 (23), 5838–5857. <https://doi.org/10.1002/cctc.v12.2310.1002/cctc.202001141>.
- Michalsky, R., Avram, A.M., Peterson, B.A., Pfromm, P.H., Peterson, A.A., 2015. Chemical Science pressure ammonia synthesis for energy storage † 3965–3974. <https://doi.org/10.1039/c5sc00789e>
- Michalsky, R., Pfromm, P.H., 2012. Thermodynamics of Metal Reactants for Ammonia Synthesis from Steam, Nitrogen and Biomass at Atmospheric Pressure 58, 3203–3213. <https://doi.org/10.1002/aic>
- Michalsky, R., Pfromm, P.H., 2011. Chromium as reactant for solar thermochemical synthesis of ammonia from steam, nitrogen, and biomass at atmospheric pressure. *Sol. Energy* 85 (11), 2642–2654. <https://doi.org/10.1016/j.solener.2011.08.005>.
- Michalsky, R., Pfromm, P.H., Steinfeld, A., 2015c. Rational design of metal nitride redox materials for solar-driven ammonia synthesis. *Interface Focus* 5, 1–10. <https://doi.org/10.1098/rsfs.2014.0084>.
- Mittemeijer, E.J., Somers, M.A., 2015. *Thermochemical Surface Engineering of Steels*. J. Chemical Information Modeling Woodhead Publishing.
- Niewa, R., 2002. Nitridocompounds of manganese: Manganese nitrides and nitridomanganates. *Zeitschrift fur Krist.* 217, 8–23. <https://doi.org/10.1524/zkri.217.1.8.20801>.
- Page, A.M., 2007. for Ordinary and Partial.
- Pfromm, P.H., 2017. Towards sustainable agriculture: Fossil-free ammonia. *J. Renew. Sustain. Energy* 9 (3), 034702. <https://doi.org/10.1063/1.4985090>.
- Rezzolla, L., 2020. Differential Equations.
- Shan, N., Chikan, V., Pfromm, P., Liu, B., 2018. Fe and Ni Dopants Facilitating Ammonia Synthesis on Mn4N and Mechanistic Insights from First-Principles Methods. *J. Phys. Chem. C* 122 (11), 6109–6116. <https://doi.org/10.1021/acs.jpcc.7b12569>.
- Shan, N., Huang, C., Lee, R.T., Manavi, N., Xu, L., Chikan, V., Pfromm, P.H., Liu, B., 2020. Manipulating the Geometric and Electronic Structures of Manganese Nitrides for Ammonia Synthesis. *ChemCatChem* 12 (8), 2233–2244. <https://doi.org/10.1002/cctc.201902383>.
- Somorjai, G.A., Zaera, F., 1982. Heterogeneous catalysis on the molecular scale. *J. Phys. Chem.* 86 (16), 3070–3078. <https://doi.org/10.1021/j100213a007>.
- Tomio, Y., Miyamoto, G., Furuhashi, T., 2016a. Precipitation Modeling in Nitriding in Fe-M Binary System. *Metall. Mater. Trans. A Phys. Metall. Mater. Sci.* 47 (10), 4970–4978. <https://doi.org/10.1007/s11661-016-3674-5>.
- Van Wigen, P.C., Rozendaal, H.C.F., Mittemeijer, E.J., 1985. The nitriding behaviour of iron-chromium-carbon alloys. *J. Mater. Sci.* 20 (12), 4561–4582. <https://doi.org/10.1007/BF00559347>.
- Vasquez, R.P., Madhukar, A., Vasquez, R.P., Madhukar, A., 1986. A kinetic model for the thermal nitridation of SiO₂/Si 234, 233–242. <https://doi.org/10.1063/1.337687>
- Wang, D., Loose, F., Chirik, P.J., Knowles, R.R., 2019. N-H Bond Formation in a Manganese(V) Nitride Yields Ammonia by Light-Driven Proton-Coupled Electron Transfer. *J. Am. Chem. Soc.* 141 (12), 4795–4799. <https://doi.org/10.1021/jacs.8b1295710.1021/jacs.8b12957.s001>.
- Zhang, J., Luo, S., Xu, C., 2010. The calculation of kinetic parameters in manganese nitriding. *Adv. Mater. Res.* 97–101, 737–742. <https://doi.org/10.4028/www.scientific.net/AMR.97-101.737>.
- Zhang, J.-Z., Xu, C.-S., Zhao, Y.-P., 2008. Kinetics of Nitrogen Diffusion in Granular Manganese. *J. Iron Steel Res. Int.* 15 (1), 85–88. [https://doi.org/10.1016/S1006-706X\(08\)60018-7](https://doi.org/10.1016/S1006-706X(08)60018-7).

Further Reading

- Heidlage, M.G., Kezar, E.A., Snow, K.C., Pfromm, P.H., 2017. Thermochemical Synthesis of Ammonia and Syngas from Natural Gas at Atmospheric Pressure. <https://doi.org/10.1021/acs.iecr.7b03173>.
- Michalsky, R., Avram, A.M., Peterson, B.A., Pfromm, P.H., Peterson, A.A., 2015b. Chemical looping of metal nitride catalysts: Low-pressure ammonia synthesis for energy storage. *Chem. Sci.* 6 (7), 3965–3974. <https://doi.org/10.1039/C5SC00789E>.
- Tomio, Y., Miyamoto, G., Furuhashi, T., 2016b. Precipitation Modeling in Nitriding in Fe-M Binary System. *Metall. Mater. Trans. A* 47 (10), 4970–4978. <https://doi.org/10.1007/s11661-016-3674-5>.